Validation of the Emission Inventory of the Year 2021 from the City of Cuenca, Ecuador, Through Weather and Air Quality Modeling Using WRF-Chem

Rene Parra *, Cristian Caguana , Claudia Espinoza

Posted Date: 19 November 2025

doi: 10.20944/preprints202511.1436.v1

Keywords: one atmosphere; modeling performance; direct effects; formal assessment

 doi:10.20944/preprints202511.1436.v1

Article

Validation of the Emission Inventory of the Year 2021 from the City of Cuenca, Ecuador, Through Weather and Air Quality Modeling Using WRF-Chem

Rene Parra [1,*], Cristian Caguana [2] and Claudia Espinoza [2]

[1] Instituto de Simulación Computacional (ISC-USFQ), Colegio de Ciencias e Ingenierías, Universidad San Francisco de Quito USFQ, Quito 170901, Ecuador

[2] Red de Monitoreo de Calidad del Aire de Cuenca, Empresa Pública de Movilidad Tránsito y Transporte de Cuenca, EMOV EP, Cuenca, Ecuador

* Correspondence: rrparra@usfq.edu.ec

Abstract

The last atmospheric emission inventory for Cuenca, a city located in the Andean region of southern Ecuador, was developed for the year 2021 (EI 2021), encompassing both primary pollutants (NO_x, CO, VOC, SO_2, PM_{10}, and $PM_{2.5}$) and greenhouse gases (CO_2, CH_4, and N_2O). We formally assessed the quality of the emission inventory by modeling air quality levels during October 2021 using the Weather Research and Forecasting with Chemistry (WRF-Chem 3.2) model at a high spatial resolution (1 km). We activated the direct effects for modeling the feedback between aerosols and atmospheric variables. The metrics indicated that both meteorological and air quality variables were modeled acceptably, suggesting the quality of the emission inventory and the ability of WRF-Chem 3.2 to perform atmospheric modeling in this complex region, using the "one atmosphere" approach. The results and spatial distribution of the EI 2021 were compared to the emission data coming from the last version of the Edgar Emissions Dataset (spatial resolution of 11.1 km) one of the most used global emission data, which suggested that for the Equatorial Andean region, the Edgar Dataset results require improvement, at least for some primary pollutants (CO, VOC, SO_2) in terms of magnitude, and of the spatial configuration of all the pollutants, before they can be used for atmospheric modeling. We also identified future research activities to improve the emission inventories and atmospheric modeling performance in the Equatorial Andean region.

Keywords: one atmosphere; modeling performance; direct effects; formal assessment

1. Introduction

Atmospheric emission inventories provide relevant information of the amount or rates of contribution of air pollutants and greenhouse gases (GHGs), produced by different sources over a specific region, for past, present, or future time [1,2]. Atmospheric emission inventories have been used both for policy and research purposes. Emission inventories provide the temporal behavior during the time, to track the reaching of goals in term of reductions of emissions [e.g, 3,4]. . On the other hand, emissions inventories provide the input for chemical transport models, which simulate the behavior of pollutants in the atmosphere for both current and hypothetical emission scenarios, as well as for atmospheric forecasting [5–7]. Emission data is probably the most important input for chemical transport models [8].

The building and use of accurate atmospheric emission inventories are directly related to some of the Sustainable Development Goals (SGDs) as the SGD 3 (Good Health and Well Being), to identify the main air pollution sources and guide air quality regulations; SDG 11 (Sustainable Cities and Communities), to support city-level policies for cleaner transport, energy, and waste management;

 doi:10.20944/preprints202511.1436.v1

and SGD 13 (Climate Action), about GHGs and other pollutants involved in the energetic balance of the atmosphere, to quantify their emissions sources and sinks, to track mitigation progress [9].

International initiatives aim to develop and make the results of emission inventories available to inform scientists and policymakers. The Edgar Emissions Database for Global Atmospheric Research is a dataset that covers time-series emission inventories for anthropogenic sources of primary pollutants and GHGs, for all countries worldwide, with a spatial resolution of up to 0.1° (approximately 11.1 km) [10]. The Edgar Emissions Database is one of the most used global atmospheric emission inventories. The CAMS emission inventory contains gridded distributions of global anthropogenic and natural emissions of atmospheric pollutants and GHGs, with resolution up to 0.1° [11].

Although emission inventories have been developed for years, they still can have high uncertainty levels [12–14]. Apart from the uncertainties inherent in emission models as simplifications of real emissions, other factors, such as the limitations of statistical data and the lack of local emission factors, can also significantly contribute. Uncertainty is also influenced by the method to downscale total emission results to a grid-cell level, accompanied by high-time resolution disaggregation, for use in a chemical transport model [15]. The assessment of uncertainty is required to clarify the usefulness and identify the sources that deserve dedicated future improvements in emission inventories [16].

The quality of an emission inventory has typically been defined by the quality of the statistical data, the emission factors, and the models used in its development. Additionally, when available, comparisons with other emission inventories have been used. Another approach to assessing the quality of an emission inventory is the use of it as input for atmospheric modeling. For this purpose, Mathias et al. (2017) [8] highlighted the need to work with accurate emissions data and provided an outlook for improving the spatial and temporal distribution of emissions inventories for use in chemical transport models. Park et al. (2023)[14] assessed emission inventories for sulfur dioxide (SO2) and oxides of nitrogen (NOx) from large point sources in South Korea, evaluating the modeling performance through a comparison of computed and recorded data for these pollutants. Malasani et al. (2024)[17] assessed five global emission inventory datasets to provide the spatial and temporal distribution of mercury over India, and also evaluated the modeling performance by comparing modeled and measured concentrations of this pollutant.

Online coupled meteorology–atmospheric chemistry models, which consider the influence and feedback between atmospheric and air quality variables, have undergone significant evolution in recent years in atmospheric modeling [18]. For this purpose, the online approach provides consistent treatment of physical and chemical processes for both numerical weather and air quality modeling, allowing the analysis through a “one atmosphere” approach. If the meteorological component is properly modeled and the comparison of the modeled air pollution levels to the corresponding records indicates consistency. In that case, we can deduce that the emission inventory is reliable and provides, although with uncertainties, useful information.

For Cuenca, a city located in the Andean region of southern Ecuador, several emission inventories have been developed since 2007. The results of the 2014 emission inventory [19] were used to conduct several modeling experiments to assess the influence of parameters and options coded in the Weather Research and Forecasting with Chemistry (WRF-Chem 3.2) model. These numerical experiments employed the online option to propose a configuration of parameters for modeling both meteorological and air quality variables, employing the “one atmosphere” approach [20,21] in urban areas of the Equatorial Andean region.

The last emission inventory for this city was created using 2021 as the base year [22], which is referred to hereafter as EI 2021. Although its uncertainty was assessed, the purpose of this contribution is to evaluate the quality and usefulness of EI 2021 by incorporating its results as input to WRF-Chem for modeling as “one atmosphere”, both meteorological and air quality variables. Additionally, the EI 2021 EI results are compared with the corresponding results from the Edgar Emissions Dataset.

 doi:10.20944/preprints202511.1436.v1

1.1. *Location and the Air Quality Network of Cuenca*

Cuenca is located in the Andean region of southern Ecuador (Figure 1), characterized by a complex topography and diverse land-use configuration. The urban area is located at 2550 masl; however, the Andes Mountains, to the west of the city, have heights exceeding 4000 masl (Figure 1c). Its air quality network has been operational since 2008, in accordance with national regulations. Currently, the air quality network is operated by the EMOV EP (Spanish acronym for Empresa Pública Municipal de Movilidad, Tránsito y Transporte de Cuenca). In the historic center of the city, an automatic station (MUN, Figure 1d) measures real-time meteorological variables (temperature, wind speed, global solar radiation, and rainfall) and air quality variables (nitrogen dioxide, NO_2; fine particulate matter, $PM_{2.5}$; and ozone, O_3). Additionally, the air quality network comprises approximately twenty passive stations, distributed throughout the city, for recording mean monthly levels of NO_2 and O_3.

Between 2012 and 2024, the MUN station measured $PM_{2.5}$ yearly mean concentrations that ranged between 5.7 and 14.5 μg m^{-3} [23], more significant than the current World Health Organization (WHO) recommendation (5.0 μg m^{-3}) [24]. Moreover, during 98 days in 2024, the 24-h mean $PM_{2.5}$ levels exceeded the current WHO guideline (15 μg m^{-3}). During 6 days in 2024, the O_3 levels exceeded the WHO guideline (100 μg m^{-3}, maximum daily mean over 8 consecutive hours). Air quality and meteorological records from the MUN station are relevant for assessing the performance of atmospheric models in Cuenca.

Additionally, for this contribution, we collected meteorological data from two meteorological stations (SAY and SOL) located west of the urban area (Figure 1c), which are operated by ETAPA EP (Spanish acronym for Empresa Pública Municipal de Telecomunicaciones, Agua Potable, Alcantarillado y Saneamiento), the entity in charge of the water management in Cuenca. Table 1 summarizes the availability of meteorological parameters for this study.

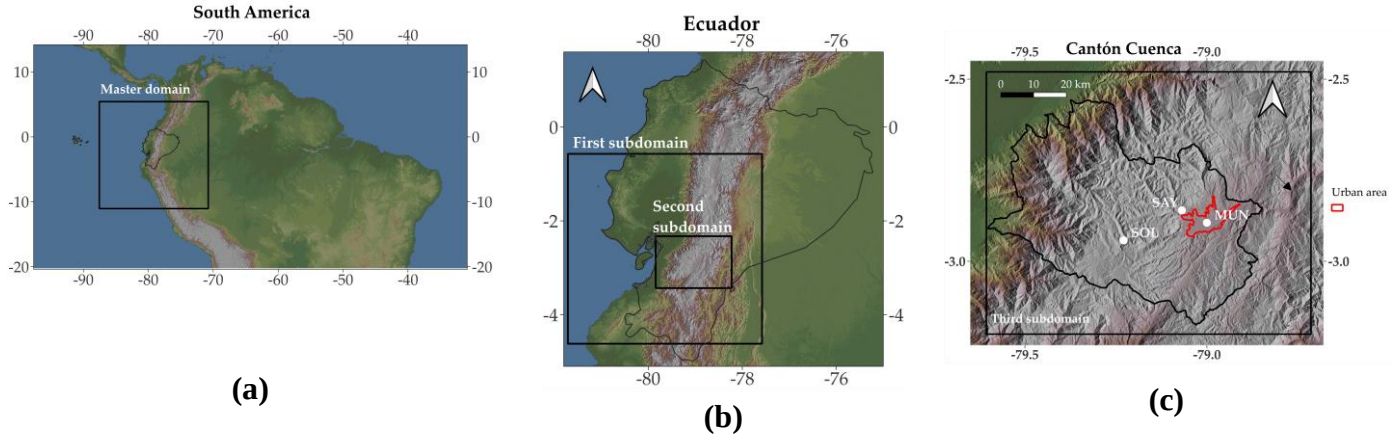

 doi:10.20944/preprints202511.1436.v1

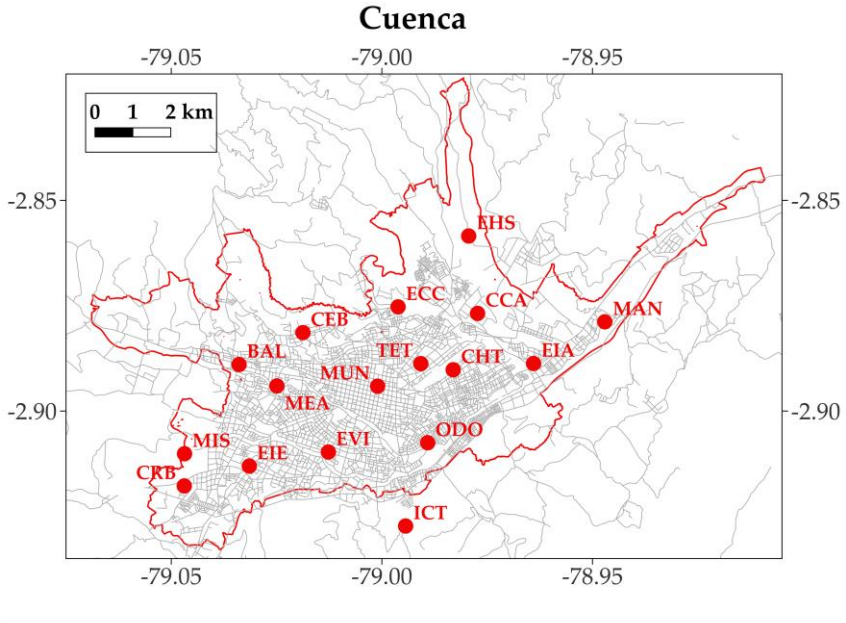

(d)

Figure 1. (a) Location of Ecuador. **(b, c)** Location of the Cantón Cuenca and meteorological stations (white dots). **(c)** The black rectangle indicates the border of the third subdomain for modeling, a grid composed of 100 columns and 80 rows. **(d)** Urban area of Cuenca (red border) and the stations of the air quality network (red dots). MUN is an automatic station for both meteorological and air quality variables. The remaining red dots indicate the locations of passive stations.

Table 1. Meteorological stations and availability of records.

Station	Nomenclature	Entity	masl	Parameters
Municipio	MUN	EMOV EP	2582	Temperature, wind speed, global solar radiation, and rainfall
Sayausí	SAY	ETAPA EP	2622	Temperature, global solar radiation, and rainfall
Soldados	SOL	ETAPA EP	3466	Global solar radiation and rainfall

1.2. The Emission Inventory of the Year 2021 (EI 2021)

The last atmospheric emission inventory for Cuenca was compiled for the year 2021, at the initiative of the EMOV EP [25], in accordance with the recommended practice of accounting for primary pollutants and GHGs [13]. Nitrogen oxides (NO_x), carbon monoxide (CO), volatile organic compounds (VOC), sulphur dioxide (SO_2), particulate matter with an aerodynamic diameter of 10 μm or less (PM_{10}), and particulate matter with an aerodynamic diameter of 2.5 μm or less ($PM_{2.5}$), were included as primary pollutants. In addition, carbon dioxide (CO_2), methane (CH_4), and nitrous oxide (N_2O) were included as GHGs.

Sources included on-road traffic, vegetation, industries, use of solvents, service stations, domestic combustion of liquid petroleum gas (LPG), use of solvents, air traffic, landfills, artisanal production of bricks, dust resuspension, and mining activities, under the territory of the Cantón Cuenca (Figure 1c). Figure 2 depicts the location of industries, service stations, landfills, and kilns used for the artisanal production of bricks.

The EI 2021 was developed to estimate real emissions in the best way possible in the territory of Cuenca, with the main goals of providing a proper emission inventory that can serve as a reference for air pollution management and the development of a future atmospheric forecasting system.

 doi:10.20944/preprints202511.1436.v1

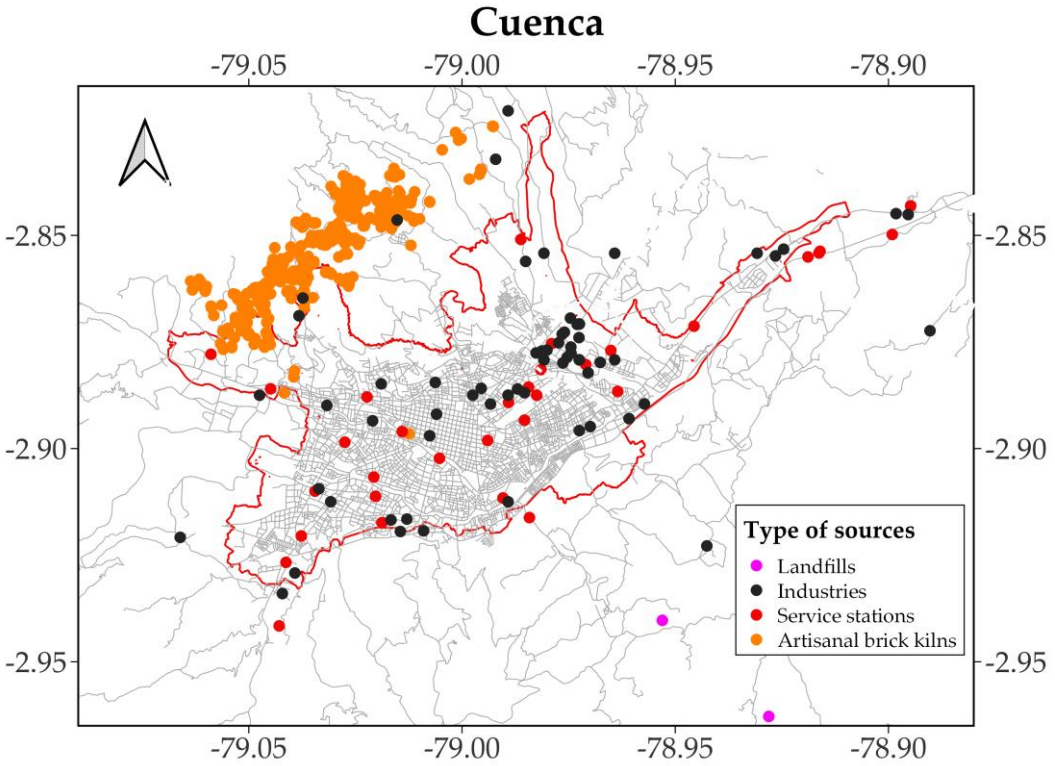

Figure 2. Location of selected types of emission sources.

Table 2. Emission Inventory of Cuenca. Primary Pollutants. Year 2021.

Source	NOx		CO		VOC		SO_2		PM_{10}		$PM_{2.5}$	
	t y^{-1}	%	t y^{-1}	%	t y^{-1}	%	t y^{-1}	%	t y^{-1}	%	t y^{-1}	%
On-road traffic	6782.4	89.8	37 624.3	95.1	4201.2	31.8	16.8	1.5	860.1	73.3	534.3	65.0
Vegetation	0.0	0.0	0.0	0.0	2813.7	21.3	0.0	0.0	0.0	0.0	0.0	0.0
Industries	555.5	7.4	286.3	0.7	176.5	1.3	1095.4	98.0	71.9	6.1	52.5	6.4
Use of solvents	0.0	0.0	0.0	0.0	4752.4	36.0	0.0	0.0	0.0	0.0	0.0	0.0
Service stations	0.0	0.0	0.0	0.0	889.2	6.7	0.0	0.0	0.0	0.0	0.0	0.0
Domestic LPG	162.2	2.1	25.3	0.1	5.4	0.0	0.0	0.0	10.7	0.9	10.7	1.3
Air Traffic	15.2	0.2	31.1	0.1	4.5	0.0	3.2	0.3	0.4	0.0	0.4	0.0
Landfills	6.3	0.1	2.6	0.0	29.5	0.2	0.0	0.0	0.1	0.0	0.1	0.0
Artisanal bricks	32.6	0.4	1577.9	4.0	341.9	2.6	2.6	0.2	226.2	19.3	223.5	27.2
Dust resuspension	0.0	0.0	0.0	0.0	0.0	0.0	0.0	0.0	0.0	0.0	0.0	0.0
Mining	0.0	0.0	0.0	0.0	0.0	0.0	0.0	0.0	4.4	0.4	0.0	0.0
Total	**7554**	**100**	**39 547**	**100**	**13 214**	**100**	**1118**	**100**	**1174**	**100**	**822**	**100**

Table 3. Emission Inventory of Cuenca. Greenhouse gases. Year 2021.

Source	CO_2		CH_4		N_2O	
	t y^{-1}	%	t y^{-1}	%	t y^{-1}	%
On-road traffic	756 655.4	66.3	203.8	4.1	83.1	83.3
Industries	229 111.8	20.1	4.3	0.1	1.6	1.6
Domestic LPG	148 890.4	13.0	2.3	0.0	10.2	10.2
Air Traffic	4737.2	0.4	0.2	0.0	0.2	0.2
Landfills	2621.3	0.2	4786.6	95.8	0.0	0.0
Artisanal bricks	53 363.7	0.0	0.2	0.0	4.7	4.7
Total	**1 142 016**	**100**	**4997**	**100**	**100**	**100**

 doi:10.20944/preprints202511.1436.v1

On-road traffic is a relevant source of emissions in Cuenca. It was estimated that about 150 800 vehicles were driven in Cuenca during 2021. Most of them (89.9%) use gasoline, while the rest (approximately 10.1%) use diesel. The presence of hybrid and electric cars was marginal. The composition of the vehicle park, in terms of percentages of used fuel, vehicle type, engine size, and year of manufacture, was deduced from statistical data of 2021 from the RTV (Spanish acronym for Revisión Técnica Vehicular), a technical control for exhaust emissions and mechanical conditions of vehicles, which has been applied in Cuenca since 2008. A survey and review of the literature were conducted to estimate the annual distances traveled and the efficiency (distance traveled per unit of fuel) by vehicle type, respectively. For consistency, the estimated fuel consumption was matched to the official statistical data on gasoline and diesel sales at Cuenca service stations for 2021. Hot, cold, and evaporative emissions were included [26], and the total results were spatially disaggregated on the emissions grid, using the intensity of the traffic map generated by EMOV EP as a proxy variable.

Vegetation is an important source of VOC. Apart from the type of vegetation and foliar biomass, the surface temperature and photosynthetically active radiation are the main physical drivers of VOC emissions from this source. For this purpose, meteorological data for 2021 were modeled for the emissions grid using the WRF model. Applying the basic model proposed by Guenther et al. [27,28], the emissions of isoprene, monoterpenes, and other volatile organic compounds were estimated.

Combustion emissions from industries were estimated using official data on fuel consumption and emission factors from the literature.

LPG is the main fuel used in the city for domestic cooking. Similarly, the combustion emissions were estimated using official data on LPG consumption and emission factors from the literature. Total yearly emissions were spatially distributed on the grid, based on a map of population density.

The emissions of VOC from service stations were estimated using official information on the sale of fuels (gasoline and diesel) in 2021. Emissions of VOC due to the use of solvents were estimated using a per-capita emission factor and the map of population density.

Emissions from landfills were estimated using the first-order decay model proposed by the IPCC [29], accounting for the amount of municipal solid waste stored at each facility, the composition of the solid waste, and the landfill's technical performance.

The yearly emissions of the primary pollutants were spatially distributed over a grid of 8000 cells (the third subdomain of the model, Figure 1c), each measuring 1 km on a side. For this purpose, the bottom-up approach was prioritized to estimate and locate the cells of emissions, complemented by the top-down approach for sources for which data are lacking and the bottom-up approach cannot be used.

More information on the emissions models for the considered sources can be found in the corresponding technical report, which shows the results of the 2021 emission inventory of Cuenca [25].

On-road traffic was the main source of NO_x (89.8%), CO (95.1%), PM_{10} (73.3%), and $PM_{2.5}$ (65%) (Table 2). Industries were the most important source of SO_2 (98.0%). The use of solvents (36.0%), on-road traffic (31.8%), and vegetation (21.3%) were the main sources of VOC. After on-road traffic, artisanal bricks contributed significantly to PM_{10} (19.3%) and $PM_{2.5}$ (27.2%) emissions. On-road traffic (66.3%), industries (20.1%), and the combustion of domestic LPG (13.0%) were the main sources of CO_2 (Table 3). Figure 2 depicts the spatial distribution of the yearly emissions of CO, NO_x, VOC, and $PM_{2.5}$.

A qualitative approach was employed to assess the uncertainty of EI 2021, using a five-category scale, ranging from A (high quality) to E (poor quality), to evaluate the quality of activity data and emission factors. Emissions by sector were classified into categories C, D, and E. The lowest grades were attributed to the quality of the emission factors [25].

Preprints.org (www.preprints.org) | NOT PEER-REVIEWED | Posted: 19 November 2025 doi:10.20944/preprints202511.1436.v1

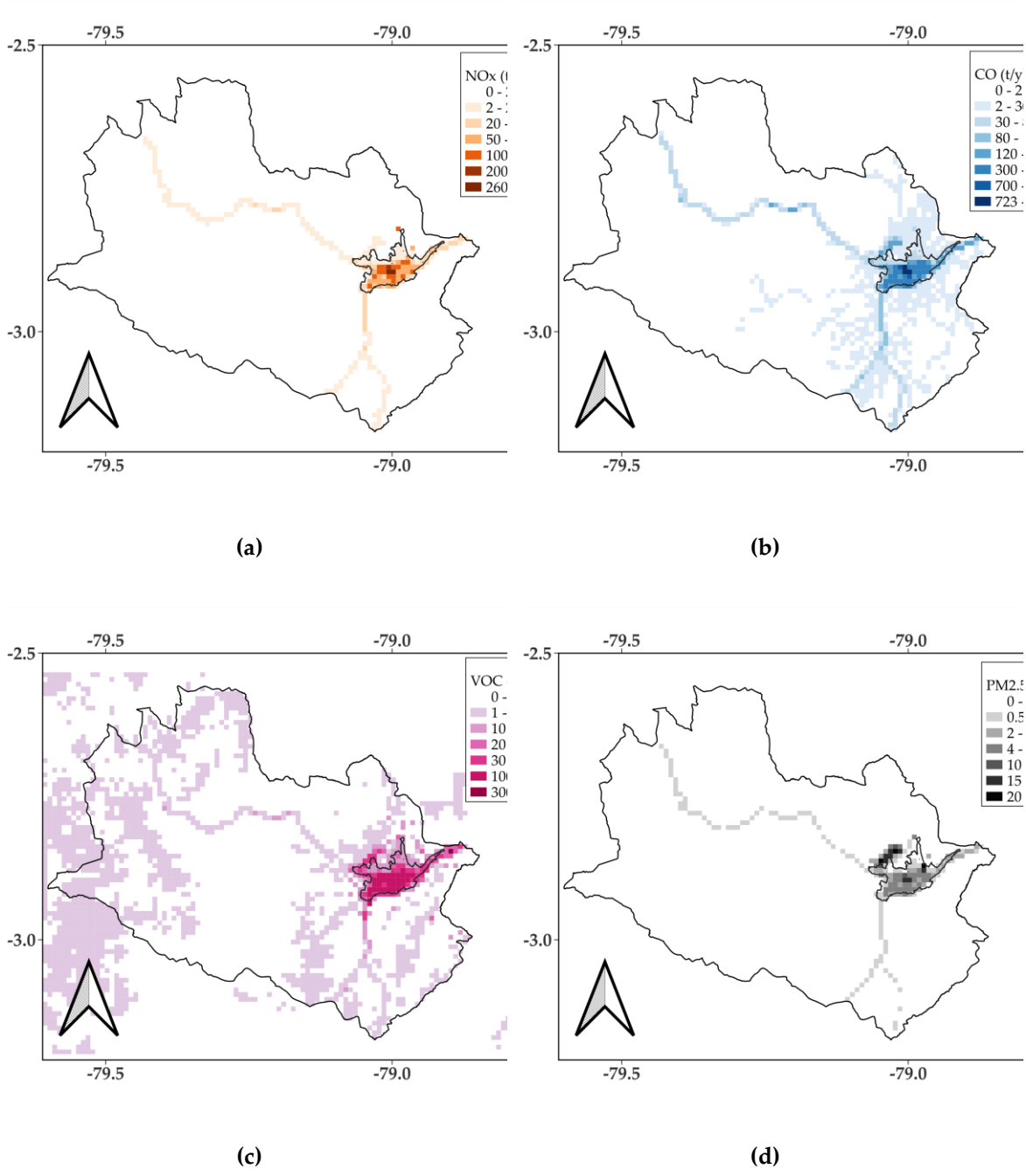

Figure 3. Spatial Distribution of the EI 2021 emissions (t y^{-1}): **(a)** CO, **(b)** NO_x, **(c)** VOC, **(d)** $PM_{2.5}$. .

2. Methods

2.1. Modeling Approach

Using Weather Research and Forecasting with Chemistry version 3.2 (WRF-Chem 3.2) [30], atmospheric modeling experiments were conducted for Cuenca to analyze the influence of parameters such as the planetary boundary layer, land surface, cumulus, and microphysics schemes [20,21]. From these studies, a configuration was recommended for modeling both atmospheric and air quality variables (Table 4). WRF-Chem is a state-of-the-art numerical 3D model used for research and forecasting purposes, enabling online analysis by considering interactions between meteorological and air quality variables through the "one atmosphere" approach.

 doi:10.20944/preprints202511.1436.v1

To test the quality of the emission inventory and considering both the availability of records and pollution conditions, we selected October 2021 for modeling. The initial and boundary conditions were generated using the Global Operational Analysis (Final, FNL) [31]. The Carbon Bond Mechanism Z (CBMZ) [32] and the Model for MOSAIC (4 sectional aerosol bins) [33] were selected to speciate and represent, respectively, the corresponding hourly emissions. The online option considers the direct effects in the feedback between aerosols and meteorological variables.

Table 4. Schemes and options for modeling [20,21].

Component	WRF variable	Option	Model and References
Cumulus Parameterization	cu_physics	0	0 No Cumulus
Microphysics	mp_physics	3	WRF Single–moment 3–class [34]
Longwave Radiation	ra_lw_physics	1	RRTM [35]
Shortwave Radiation	ra_sw_physics	2	Goddard [36]
Surface Layer	sf_sfclay_physics	1	MM5 similarity [37]
Planetary Boundary Layer	bl_pbl_physics	1	Yonsei University [38]
Land Surface	sf_surface_physics	2	Noah [reference] [39]
Urban surface	sf_urban_physics	0	No urban physics
Chemical mechanism and aerosol modules	chem_opt	7	CBMZ and MOSAIC [32,33]

2.2. *Metric of Modeling Performance*

We assessed the performance of the model in predicting surface temperature and wind speed using the following metrics: gross error (GE), mean bias (MB), index of agreement (IOA), and root mean square error (RMSE), as described in Table 5. The equations and accuracies for these metrics are described in the guide by the European Environment Agency [40].

The performance of the model for daily rainfall was assessed by the percentage of equation (1).

$$Pdcm = \frac{Ndr+Ndwr}{Tmd}.100, \quad (1)$$

Pdcm: Percentage of days with or without rainfall captured by modeling.

Ndr: Number of days with rainfall (≥ 0.2 mm d^{-1}) in agreement between records and modeled rainfall.

Ndwr: Number of days without rainfall (< 0.2 mm d^{-1}) in agreement between records and modeled rainfall.

Tmd: Total modeled days

The intensity of 0.2 mm d^{-1} identifies a rainy day or a day with measurable precipitation [41]. For days without rainfall, we considered that the model captured the record if both were < 0.2 mm d^{-1}. For days with rainfall, we considered the model to be in agreement with the corresponding record if both values were ≥ 0.2 mm d^{-1}.

For assessing the short-term air quality modeling performance, we used the records of nitrogen dioxide (NO_2), $PM_{2.5}$, and O_3 from the MUN station, using the periods of time (Table 5) defined by the national regulation and the World Health Organization guidelines [24,42,43], to compute the MB, RMSE, the fractional bias (FB), the mean normalized bias (MNB), and the correlation coefficient (r).

For assessing the long-term air quality modeling, the performance was evaluated as the percentage of passive stations that showed a maximum difference of up to 30% between the modeled monthly concentration and the recorded data.

Additionally, we calculated the percentages of records captured by modeling, based on the accuracy presented in Table 5.

 doi:10.20944/preprints202511.1436.v1

Table 5. Metrics for modeling atmospheric variables [40,44].

Variable	Metric	Benchmark or Ideal Range	Accuracy
Hourly surface temperature	GE	<2 °C	±2 °C
	MB	(-0.5 °C, 0.5 °C)	
	IOA	≥0.8	
Hourly wind speed (10 mas)	RMSE	<2 m s^{-1}	±1 m s^{-1}
	MB	(-0.5 m s^{-1}, 0.5 m s^{-1})	
	IOA	≥0.6	
Daily air quality: Max. 1-h NO_2, 24-h $PM_{2.5}$ mean, max. 8-h O_3 mean	MB	0	±50%
	RMSE	0	
	FB	0	
	MNB	0	
	r	1	
Monthly air quality: NO_2 and O_3			±30%

2.3. *Processing of the Data from the Edgar Emissions Database*

For comparison purposes, we identified and extracted the information of the cells of the global domain of the Edgar Emissions Database (EDGARv8.1) [4,10,15,45] mesh within the territory of the Cantón Cuenca (Figure 1c). We geoprocessed the 2021 data and totaled the emissions from these cells, for the primary pollutants and GHGs considered in the EI 2021.

3. Results

3.1. *Meteorology*

At the MUN stations, the modeled surface temperature reached values within the expected benchmark range for GE and IOA (Table 6), capturing the trend observed in records (Figure 4a). However, at the SAY station, only IOA was in range. For both stations, a strong relationship was observed between the records and modeled hourly temperatures (IOA ≥ 0.8).

At the MUN station, although the model showed an overestimation during the afternoon (Figure 4b), the wind speed was accurately modeled, as all the metrics fell within the expected range (Table 6).

The model captured 78.4% and 60.3% of the hourly temperature records at the MUN and SAY stations, respectively (Table 7). Most of the wind speed records (75.8%) were properly modeled at the MUN station.

Daily rainfall records were best captured at the SAY station (80.0%), followed by the SOL station (73.3%) and the MUN station (46.7%) (Table 7).

From 1 to 30 October 2021, 19 days had no rainfall or intensities lower than or equal to 0.2 mm d^{-1} at the MUN station (Figure 5a). Eleven days showed measurements between 0.4 to 21.0 mm d^{-1}. In comparison, the model quantified 13 days with no rainfall or intensities lower than or equal to 0.2 mm d^{-1}, and 17 days with intensities between 0.4 to 30.5 mm d^{-1}. A better agreement was obtained at the SAY station, which had 20 days without rainfall or with rainfall intensities lower than or equal to 0.2 mm d^{-1}, similar to the days quantified by the modeling. At the SOL station, which is located over the Andean mountains, the model indicated that all the days (30) had intensities higher than 0.2 mm d^{-1}, although the records indicated 22 days. At the three stations, the ranges of the modeled rainfall were consistent with the ranges of the records.

The global solar radiation at the MUN (Figure 4c), SAY (not shown), and SOL (not shown) stations was overestimated.

 doi:10.20944/preprints202511.1436.v1

Table 6. Metrics for modeling meteorological variables.

Metric	MUN	SAY	Benchmark
Hourly surface temperature:			
GE	**1.46**	2.11	**<2 °C**
MB	0.61	0.74	**(-0.5 °C, 0.5 °C)**
IOA	**0.84**	**0.86**	**≥0.8**
Hourly wind speed:			
RMSE	**1.04**	NA	**<2 m s^{-1}**
MB	**0.31**	NA	**(-0.5 m s^{-1}, 0.5 m s^{-1})**
IOA	**0.72**	NA	**≥0.6**

NA: Not assessed.

Table 7. Percentage of records captured by modeling meteorological variables.

Parameter	MUN	SAY	SOL
Hourly surface temperature	78.4	60.3	NA
Hourly wind speed	75.8	NA	NA
Daily rainfall	46.7	80.0	73.3

NA: Not assessed.

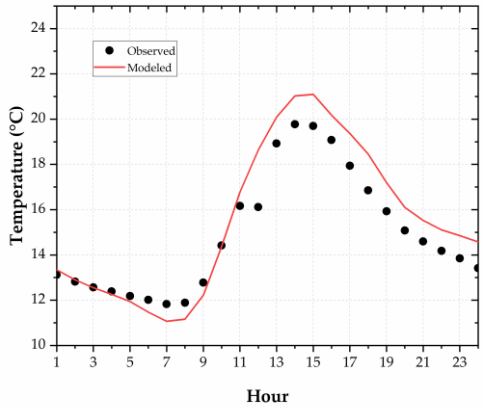

(a)

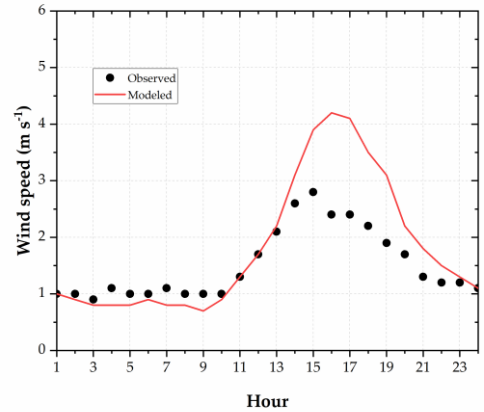

(b)

Preprints.org (www.preprints.org) | NOT PEER-REVIEWED | Posted: 19 November 2025 doi:10.20944/preprints202511.1436.v1

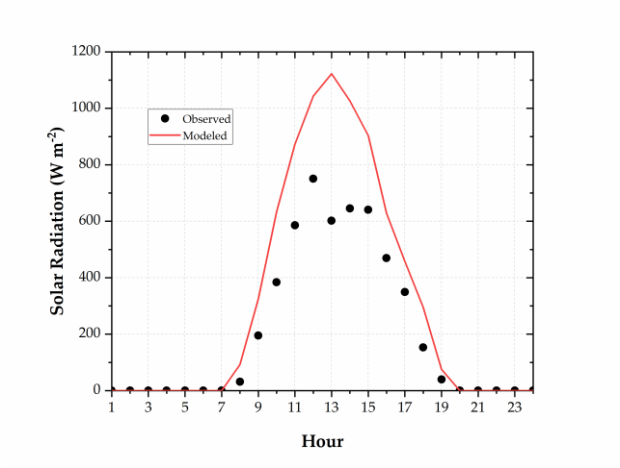

(c)

Figure 4. MUN station. Daily mean profiles during October 2021: (**a**) Surface temperature. (**b**) Wind speed. **(c)** Global solar radiation.

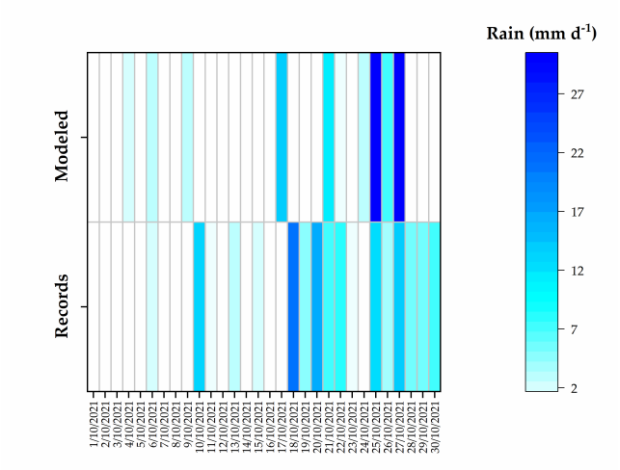

(a)

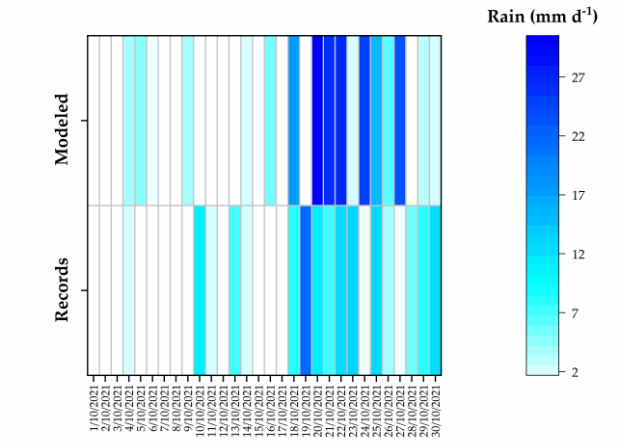

(b)

 doi:10.20944/preprints202511.1436.v1

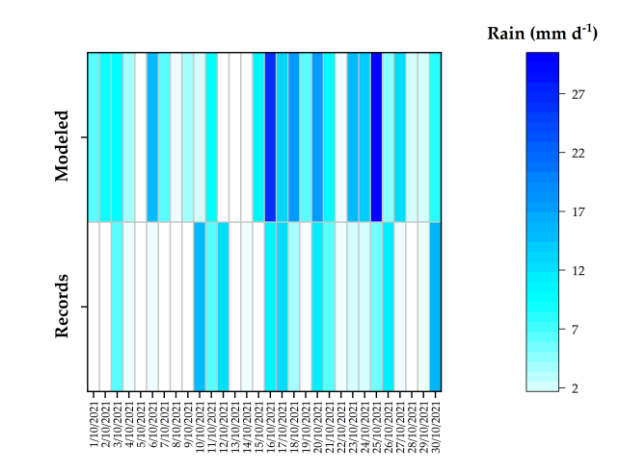

(c)

Figure 5. Rainfall records and modeled values: **(a)** MUN. **(b)** SAY. **(c)** SOL.

3.2. Air Quality

Although the model provided a consistent mean daily profile with the records, it slightly overestimated the maximum 1 h NO_2 levels (MB = 7.9 μg m^{-3})(Table 8, Figure 6a,b). However, the model showed no strong linear relationship between the recorded and modeled values (r = 0.3). On the contrary, the model slightly underestimated the mean 24 h $PM_{2.5}$ levels (MB = -3.4 μg m^{-3}) and, similarly, showed a weak relationship between records and computed levels (r = -0.12). Although with a positive bias (MB = 14.4 μg m^{-3}), the model provided a consistent mean daily profile of O_3 levels compared to records and showed a good linear relationship (r = 0.61).

The model captured 80.0%, 76.7%, and 66.7% of the maximum 1 h daily NO_2, 24 h $PM_{2.5}$ mean, and maximum 8 h O_3 daily mean, respectively (Table 9).

Although with differences, the model provided consistently mean daily profiles for the three assessed pollutants compared to records (Figure 6b, d, f). On average, although the model fitted the hourly O_3 concentrations during the morning, it overestimated them at midday and in the afternoon (Figure 6f).

At the passive stations, the NO_2 and O_3 monthly mean concentrations were properly modeled at 81.3% and 76.5%, respectively (Table 9, Figure 7).

Table 8. Short-term air quality metrics.

		Ideal Value
Maximum 1 h NO_2 mean:		
MB	7.9	0
RMSE	15.9	0
FB	14.6	0
MNB	22.1	0
r	0.3	1
24 h $PM_{2.5}$ mean:		
MB	-3.40	0
RMSE	5.33	0
FB	-29.2	0
MNB	-21.00	0
r	-0.12	1
Maximum 8 h O_3 mean:		
MB	14.39	0
RMSE	18.74	0
FB	25.9	0

 doi:10.20944/preprints202511.1436.v1

MNB	41.48	0
r	0.61	1

Table 9. Percentage of records captured by modeling air quality variables.

Short-term air quality:	
Max. 1 h NO_2 mean	80.0
24 h $PM_{2.5}$ mean	76.7
Max. 8 h O_3 mean	66.7
Average:	74.5
Long-term air quality:	
NO_2, monthly mean	81.3
O_3, monthly mean	76.5
Average:	78.9

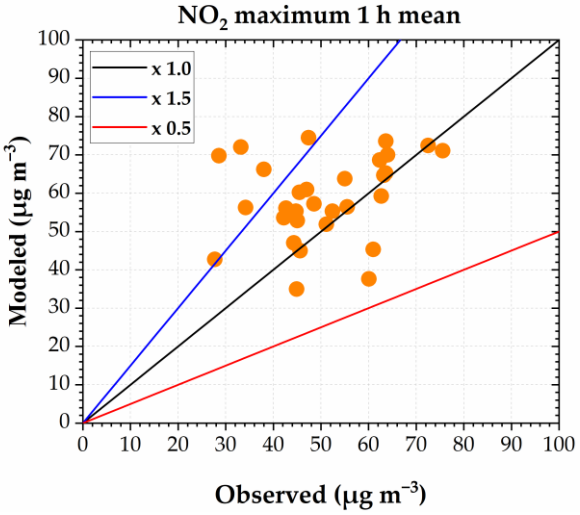

(a)

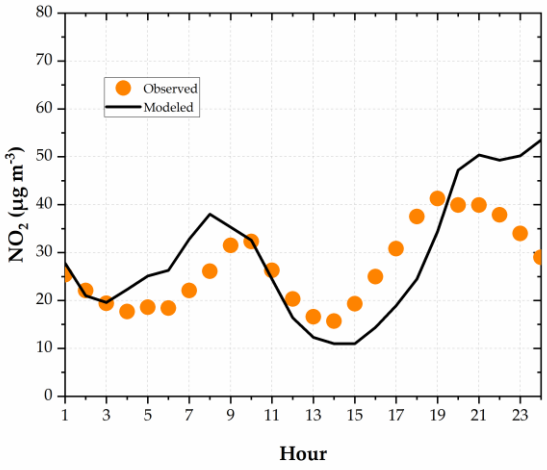

(b)

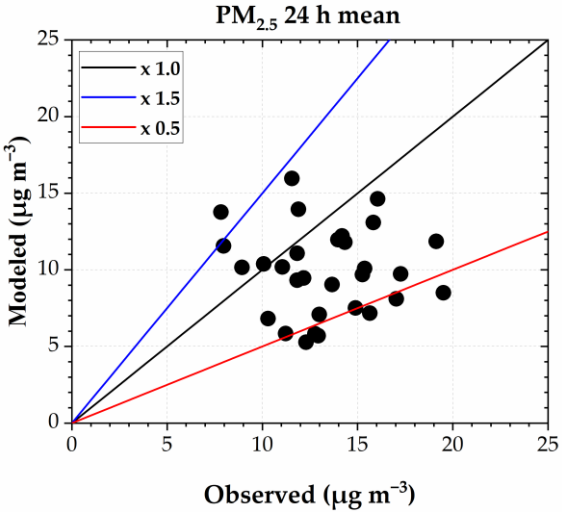

(c)

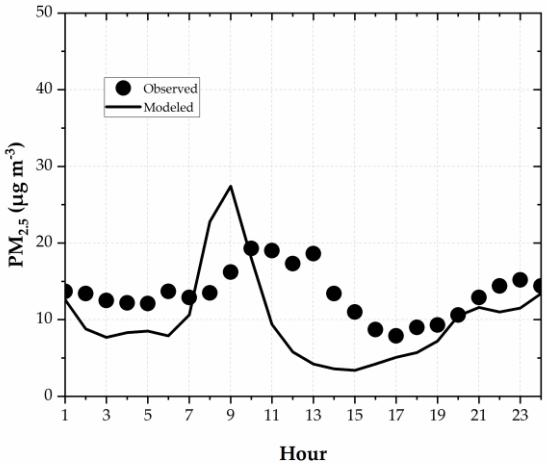

(d)

 doi:10.20944/preprints202511.1436.v1

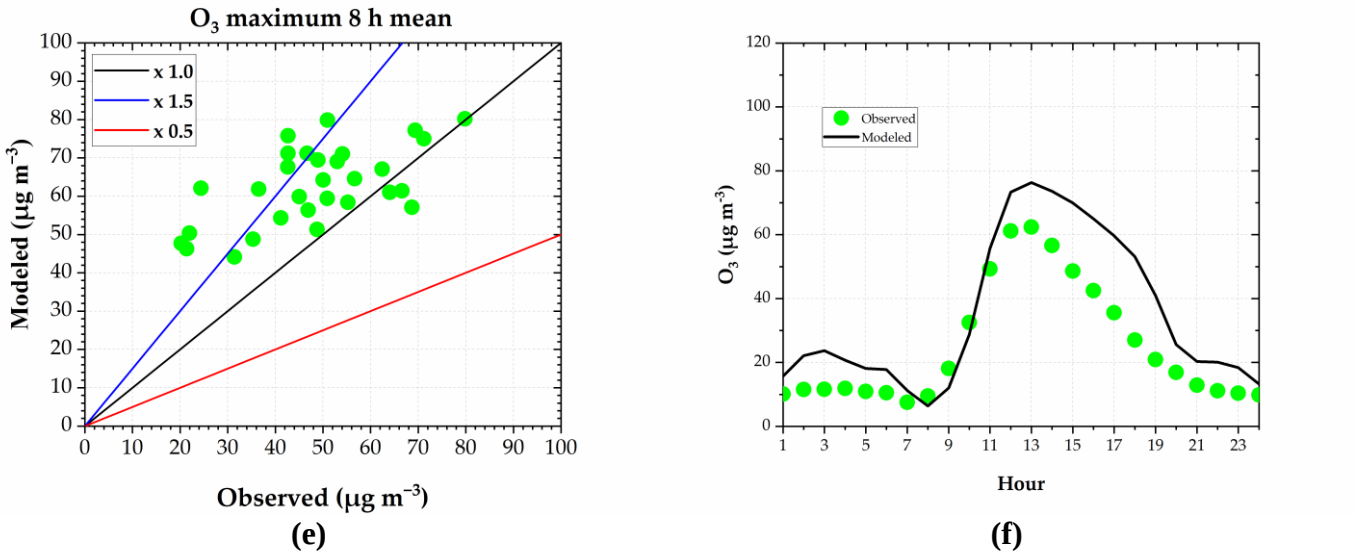

Figure 6. Observed versus modeled daily concentrations: **(a)** NO_2 1 h maximum; **(b)** Mean daily profiles of hourly NO_2; **(c)** $PM_{2.5}$ 24 h mean; **(d)** Mean daily profiles of hourly $PM_{2.5}$; **(e)** O_3 8 h maximum; (**f**) Mean daily profiles of hourly O_3.

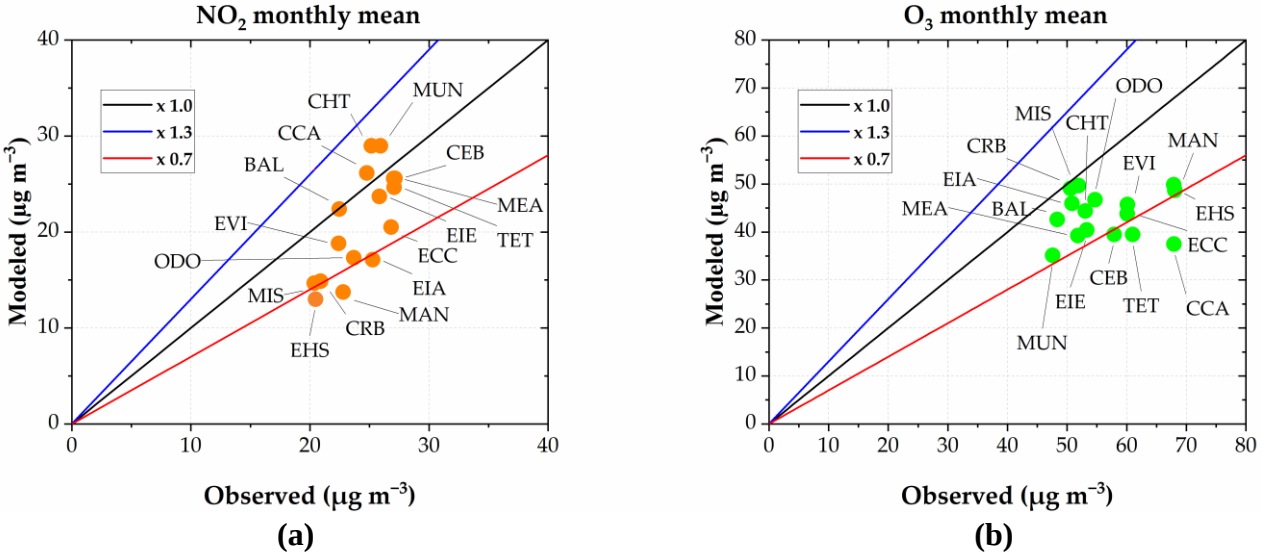

Figure 7. Observed versus modeled levels at passive stations: (**a**) NO_2 and (**b**) O_3.

As an example of modeled air quality variables, Figure 8 illustrates the spatial configuration of the modeled $PM_{2.5}$ levels on 17 Oct 2021, which ranged between 3 and 45 µg m^{-3}. The highest levels were computed at the north and northwest of the urban area, between 04:00 and 07:00 L.T., corresponding to the influence of the emissions from artisanal brick kilns (Figure 2). The concentrations decreased with atmospheric warming during daylight hours and increased again during the night, reaching up to 20 µg m^{-3} at 22:00 L.T. over the urban area.

Figure 9 shows the map of modeled O_3 levels on 17 Oct 2021. The highest levels were computed at the northwest and west, outside the urban area, between 11:00 and 13:00 L.T., reaching levels up to 130 µg m^{-3}. Over the urban area, at midday, the O_3 levels reached 100 µg m^{-3}.

 doi:10.20944/preprints202511.1436.v1

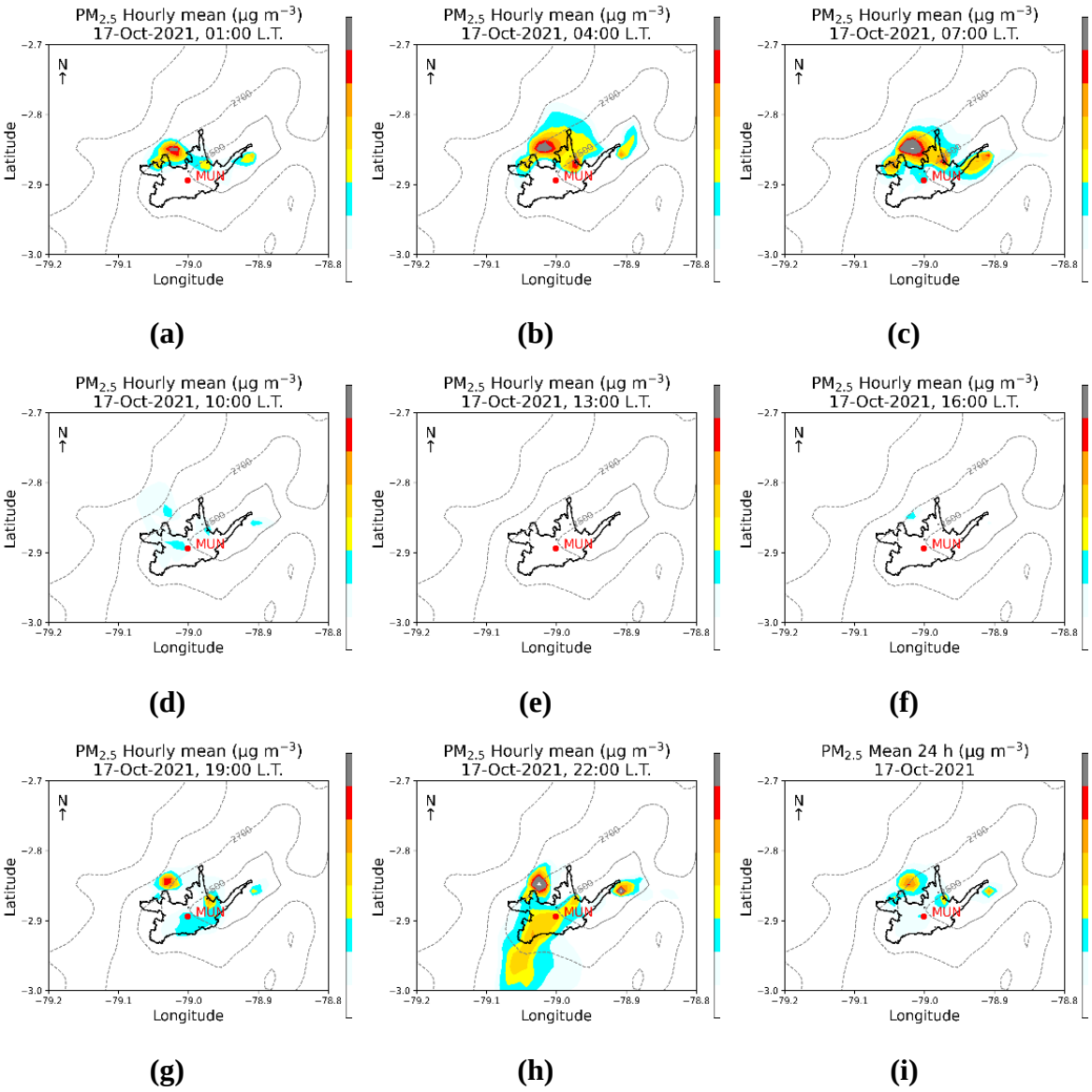

Figure 8. Modeled $PM_{2.5}$ levels for 17 Oct 2021. Results in local time (L.T.). Hourly mean concentrations: **(a)** 01:00, **(b)** 04:00, **(c)** 07:00, **(d)** 10:00, **(e)** 13:00, **(f)** 16:00, **(g)** 19:00, **(h)** 22:00. **(i)** Mean concentration during 24 h.

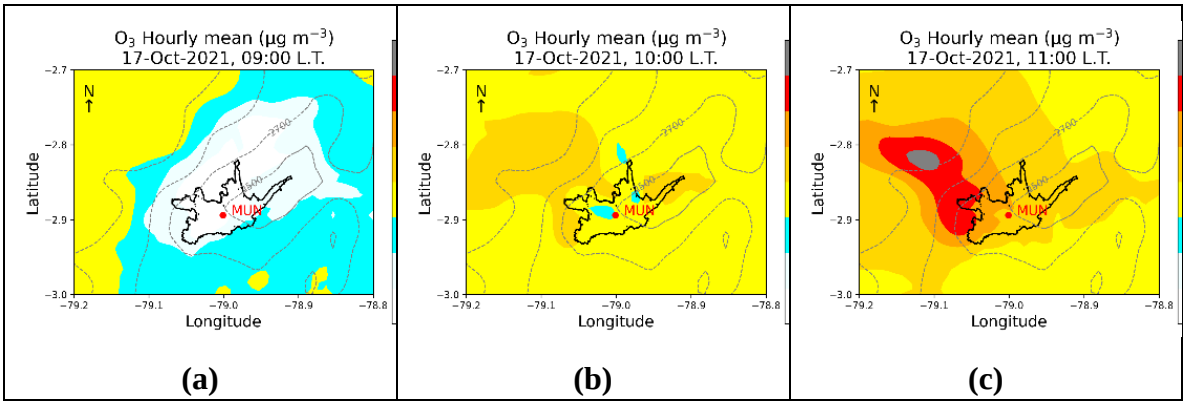

 doi:10.20944/preprints202511.1436.v1

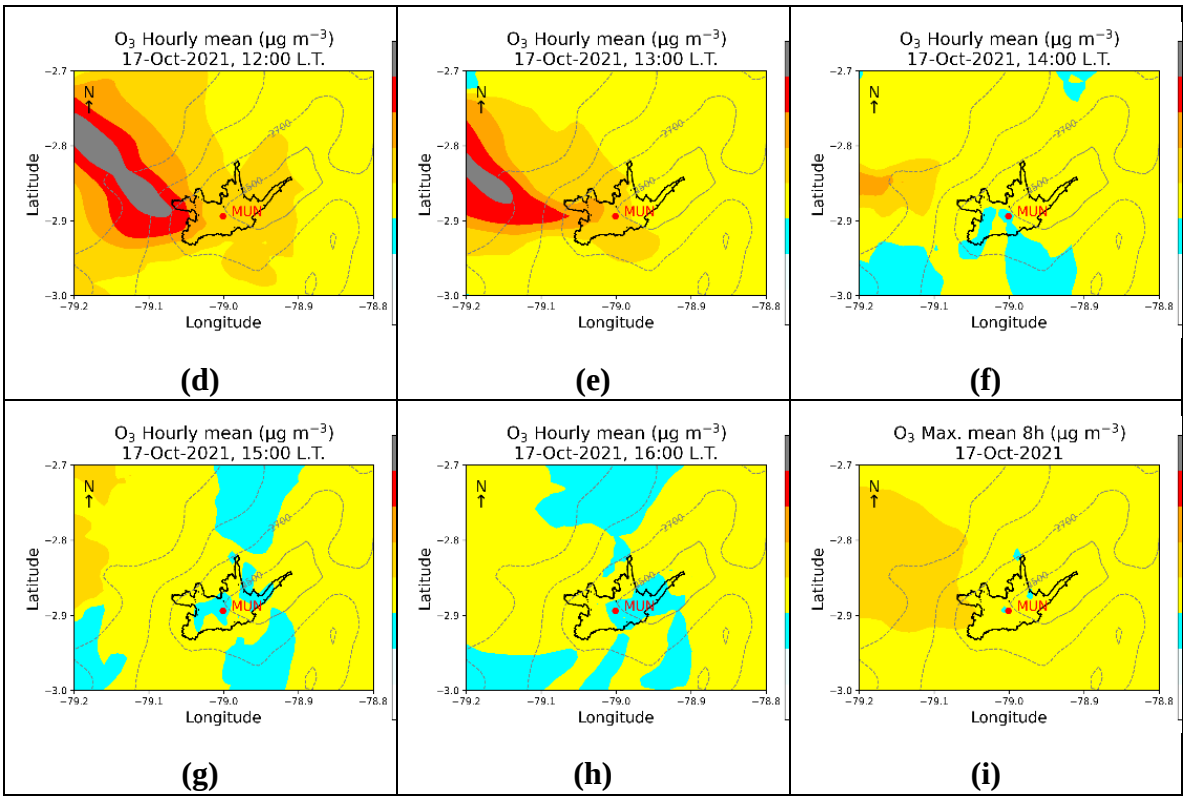

Figure 9. Modeled O_3 levels for 17 Oct 2021. Results in local time (L.T.). Hourly mean concentrations: **(a)** 09:00, **(b)** 10:00, **(c)** 11:00, **(d)** 12:00, **(e)** 13:00, **(f)** 14:00, **(g)** 15:00, **(h)** 16:00. **(i)** Maximum mean concentration during 8 h.

3.3. Comparison to the Edgar Emissions Dataset

Table 10 compares the EI 2021 results with the emissions for the same year from last version of the Edgar Emissions Dataset [10]. The total NO_x emissions were consistent, with a ratio of 1.13 between the EI 2021 value to the Edgar Dataset. Higher differences were observed for CO and VOC emissions, with ratios of 1.72 and 2.66, respectively. The SO_2 and $PM_{2.5}$ emissions of EI 2021 were about 30% and 66% respectively, of the values from the Edgar Dataset.

The CO_2 emissions were consistent, with a ratio of 1.14 between the EI 2021 value and the estimated value from the Edgar Dataset. Higher differences resulted for CH_4 and N_2O, with ratios of 0.46 and 0.26, respectively. The ratio of total CO_2-equivalent emissions was 0.93. The per capita GHGs emissions were consistent, with values of 2.01 t CO_2 eq. per capita y^{-1} for EI 2021, and 2.16 t CO_2 eq. per capita y^{-1}, for the Edgar Dataset.

For the estimation of the GHGs emissions in units of CO_2 equivalent, we used 27 and 273, for the global warming potential of CH_4 (mostly non-fossil) and N_2O, respectively, taken from the sixth Intergovernmental Panel on Climate Change (IPCC) report [46].

Figure 10 depicts the spatial distribution of total CO emissions. The EI 2021 map, with a 1 km spatial resolution, provides a more accurate depiction of the emissions distribution. The map generated from the Edgar Dataset, with a resolution of approximately 11.1 km, provides coarser and even mislocated emissions, as observed for the other pollutants as well (no-show).

Table 10. Comparison to the results from the Edgar Emissions Dataset. Year 2021.

	EI 2021 (a)	Edgar Dataset (b)	Ratio a/b
Primary pollutants	(t y^{-1})	(t y^{-1})	
NO_x	7554	6690	1.13
CO	39 547	22 986	1.72
VOC	13 214	4970	2.66

 doi:10.20944/preprints202511.1436.v1

SO_2	1118	3851	0.29
PM_{10}	1174	1558	0.75
$PM_{2.5}$	822	1237	0.66
GHGs	(t y^{-1})	(t y^{-1})	
CO_2	1 142 016	1 004 333	1.14
CH_4	4997	108 15	0.46
N_2O	100	392	0.26
Total GHGs	(t CO_2 eq. y^{-1})	(t CO_2 eq. y^{-1})	
CO_2 eq.	1 304 235	1 403 332	0.93
GHGs emission per capita:	(t CO_2 eq. per capita y^{-1})	(t CO_2 eq. per capita y^{-1})	
CO_2 eq. per capita	2.01	2.16	0.93

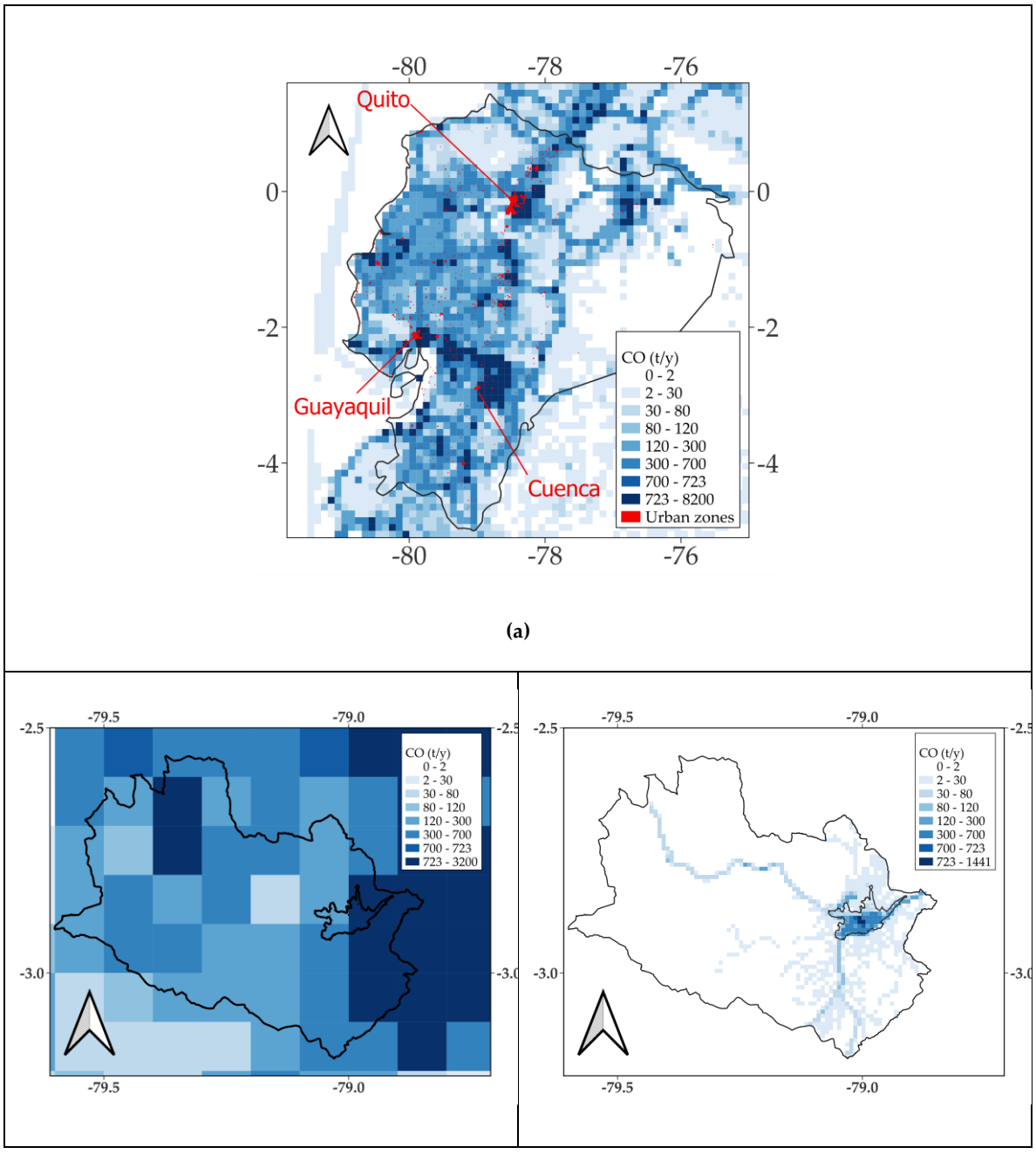

(a)

 doi:10.20944/preprints202511.1436.v1

(b)	(c)

Figure 10. Spatial distribution of the CO emission for the year 2021: **(a)** Ecuador, Edgar dataset (spatial resolution: 11.1 km). **(b)** Cuenca, Edgar dataset (spatial resolution 11.1 km). **(c)** Cuenca, EI 2021 (spatial resolution: 1 km).

4. Discussion and Conclusions

We assessed the quality of the EI 2021 emission inventory from Cuenca by using it as input to the WRF-Chem model to simulate atmospheric and air quality variables at a high spatial resolution (1 km). To our knowledge, this is the first time that an atmospheric emission inventory from the Equatorial Andean region has been formally assessed by atmospheric modeling of meteorological (surface temperature, surface wind speed, and total daily rainfall) and air pollution variables (maximum 1 h NO_2 mean per day, mean 24 h $PM_{2.5}$, maximum 8 h O_3 mean per day, monthly mean levels of NO_2 and O_3). We utilized a state-of-the-art tool that models the direct effects of aerosols on meteorological variables. The results indicated that both meteorological and air quality variables were acceptably modeled, suggesting the quality of the EI 2021 emission inventory and WRF-Chem's ability to model the atmosphere as a unique system [13,47].

The comparison of the EI 2021 results with the corresponding emissions from the Edgar Dataset indicated a good agreement for NOx. In both cases, transportation and industry were identified as the main sources of NO_x.

The CO emissions from the EI 2021 were 1.7 times higher than those from the Edgar Dataset, despite the latter including other sectors, such as agricultural activities. We hypothesize that the difference can be partly explained by Cuenca's geographical altitude (2550 masl). Molina and Molina reported that, at 2240 masl, the Mexico City Metropolitan Area has 23% less oxygen (O_2) than at sea level [2]. Similarly, at the height of Cuenca, the lower O_2 availability affects combustion processes, leading to higher atmospheric emission factors of primary pollutants [48,49].

The VOC emission from EI 2021 was 2.7 times higher than the estimate from the Edgar Dataset. Although there is significant uncertainty in VOC emissions, the main reason for the difference could be that the Edgar Dataset covers human-made sources, whereas the EI 2021 also includes VOC emissions from vegetation.

The SO_2 emission by the EI 2021 was about 29% of the Edgar estimation. In both cases, industry and transportation were identified as the primary sources of SO_2. As the EMOP EV conducted a dedicated sampling campaign in service stations to characterize the sulfur content of the fuels delivered in Cuenca during 2021, we considered the EI 2021 estimate to be more reliable.

The PM_{10} and $PM_{2.5}$ emissions from EI 2021 were 75% and 66% of the estimates from the Edgar Dataset, respectively. These ratios seem consistent, as the EI 2021 did not include emissions from agricultural activities.

The comparison of the EI 2021 results with the corresponding emissions from the Edgar Dataset indicated a good agreement for CO_2. Important differences were identified for CH_4 and N_2O. The primary purpose of the EI 2021 was, in addition to VOCs from vegetation, to focus on combustion and fugitive emissions from human-made sources. Therefore, the EI 2021 did not include CH_4 sources from enteric fermentation, agricultural or livestock activities, nor N_2O sources from fertilizer use, both of which were included in the Edgar Dataset, in agreement with the IPCC method.

High levels of uncertainty still characterized the emission inventories [13]. For the case of the EI 2021, we identified different components that deserve dedicated improvements in the future. In addition to the quality required for the activity data, defining its own emission factors is a priority for the Equatorial Andean region, considering the influence of the decrease in oxygen in the atmosphere with increasing height above sea level, which in turn increases the magnitude of primary pollutant emissions such as CO, VOC, and particulate matter. For countries like Ecuador, in general, there are very few own emission factors, and currently, most of them are taken from the international literature, which is established mostly for locations at sea or at low heights above sea level.

 doi:10.20944/preprints202511.1436.v1

The EI 2021, although with uncertainties, is a valuable contribution in terms of describing the most important sources of primary pollutants and GHGs in Cuenca. The corresponding results can be used as a reference to explore options to improve the air quality, as the change of the composition of the vehicle park, the promotion of electric vehicles, the benefits in terms of the improvement of the fuels' quality, or the expected health benefits due to the use of exhaust filter particles in diesel vehicles. Additionally, the EI 2021 serves as a proper reference for environmental impact assessments of policies, programs, and projects that affect air quality. Even, the EI 2021 results could be used to explore the modeling performance of a preliminary atmospheric forecasting system.

In the future, to reduce the uncertainty of emission inventories in Cuenca, we identified the following activities:

For on-road traffic, as one of the most important sources of both primary pollutants and GHGs, it is essential to improve and keep updated a map of daily traffic intensities for avenues, roads, and main streets. If possible, collect data to describe the characterization of the type and number of vehicles on the avenues and roads with the highest levels of traffic. For this purpose, traffic counting supported by cameras should be implemented. Another option could be the access and analysis of data describing the dynamic behavior of passengers' cell phones as a proxy variable to infer the distribution of daily and hourly on-road traffic behavior.

The RTV (Spanish acronym for Revisión Técnica Vehicular) is a technical control for exhaust emissions and mechanical conditions of vehicles, which has been applied in Cuenca since 2008. According to national regulations, it is a prerequisite for the legal use of each vehicle throughout the year. Currently, the RTV controls the hydrocarbon and carbon monoxide exhaust emissions for gasoline vehicles, as well as opacity, a measurement of how much light is blocked by particulate matter, for diesel vehicles.

The database generated by the RTV control is a valuable resource, which was used to characterize the composition of the city's vehicle park. This dataset can include the record of the distance traveled per vehicle each time it is tested annually. This information will enable a more accurate estimation of the distance traveled per year, thereby improving the accuracy of the on-road activity data.

Additionally, it is necessary for each type of vehicle to maintain and update the information on the distance traveled per unit of consumed fuel. For this purpose, apart from the information provided by the vehicle makers, it is advisable to conduct dedicated surveys of vehicle owners who can provide consistent information on the conditions in Cuenca.

Due to both short-term and long-term exceedances of the WHO guidelines [23], determining local PM2.5 emission factors is a priority, particularly for diesel vehicles and fixed sources that use fossil fuels and biomass. The RTV should additionally include the control of the exhaust emissions of $PM_{2.5}$ and NO_x for diesel cars. In fact, the RTV database of the exhaust emission measurements (e.g., [50–52]) should be used to deduce local emission factors as a complement to the results from in-route use of on-board measurement devices (e.g., [53–55]). Particularly, the viability of deducing $PM_{2.5}$ emission factors from opacity records deserves dedicated research, as the literature reports correlated or weak correlations (e.g., [56,57]).

Also, it is necessary to define local emissions factors for the NO_x and VOC, as precursors of O_3. Particularly, it is necessary to characterize local VOC emission factors from gasoline vehicles, vegetation, service stations, and the use of solvents.

Regarding VOC emissions from vegetation, practically no national or local emission factors are available. Additionally, some native species lack information on their VOC emission capacity. Therefore, determining their emission factors [58,59] is a priority field of research. Particularly, vegetation is a source with high emission uncertainty. In the future, it will be necessary to have an improved characterization of the spatial configuration of species and of the foliar biomass, as well as its dynamics throughout the annual cycle.

For future emission inventories, as a good practice, other components can be added, such as the quantification of black and elemental carbon [24].

 doi:10.20944/preprints202511.1436.v1

In general, the availability of atmospheric records is low in the Andean Region of Ecuador [60,61]. Particularly, the promotion of vertical sounding of meteorological and air quality species will enhance the characterization of parameters, such as the planetary boundary layer height and the vertical abundance of species, thereby providing useful information for improving the generation of the boundary conditions for modeling purposes and allowing a more complete assessment of the modeling performance by the inclusion of vertical comparisons.

The EI 2021 provided a useful spatial distribution of emissions (resolution of 1 km), as can be inferred from the modeling performance. Apart from the differences in emissions for some primary pollutants, the comparison with the emissions from the Edgar Dataset indicated that the latter is still too coarse (resolution of 11.1 km) for modeling purposes at the required scale for Equatorial Andean cities, such as Cuenca.

One of the advantages of the Edgar Dataset is its consistent use of the same method, although this approach may overlook country-specific details that could enhance the emission estimates and their spatial distribution [8]. The Edgar Dataset, one of the most widely used emission resources. Georgiou et al. (2022)[7] reported the performance of an atmospheric forecasting system applied over the Eastern Mediterranean, based on the emission from the Edgar Dataset and the WRF-Chem, assessing the modeling performance of both meteorological and air quality parameters. Yarragunta et al. (2025) [62] utilized the Edgar Dataset as input to WRF-Chem for atmospheric modeling, similarly assessing the performance of meteorological and air quality quantities. However, our results and comparison to the EI 2021 suggest that for the Equatorial Andean region, the Edgar Dataset results require improvement, at least for some primary pollutants (CO, VOC, SO2) in terms of their magnitude and of the emission spatial configuration of all the pollutants, before they can be used for atmospheric modeling. Their results can be used to generate emissions, possibly using proxy variables, with a high spatial resolution (1 km), which allows for adequate emissions for atmospheric modeling in cities located in the equatorial zone of the Andes.

To assess the quality of the EI 2021, we used version 3.2 of the WRF-Chem model, as had been previously tested in Cuenca to define a recommended configuration of options, which was used in the present contribution. However, there are modeled results for both meteorological and air quality variables that can be improved. For example, the model overestimated global solar radiation, which in part explains the overestimation of O_3 levels during the afternoon. New versions and configurations of the WRF-Chem model can be tested to identify a scheme, if any, that improves the modeling of cumulus processes, thereby enhancing the representation of cloud coverage, rainfall, and surface solar radiation. Similarly, the potential benefits from the activation for indirect effects between aerosols and meteorological variables need to be assessed.

Author Contributions: Conceptualization, R.P.; methodology, R.P.; air quality and meteorological monitoring, C.G., and C.E., data curation, C.G., and C.E.; modeling, R.P.; validation, R.P., C.G., and C.E.; writing—original draft preparation, R.P.; writing—review and editing, R.P., C.G., and C.E. All authors have read and agreed to the published version of the manuscript

Funding: This research received no external funding.

Institutional Review Board Statement: Not applicable.

Informed Consent Statement: Not applicable.”
Data Availability Statement: Not applicable.

Acknowledgments: This research is part of the "Emisiones atmosféricas y Calidad del Aire en el Ecuador 2026" project. Simulations were done at the High-Performance Computing system at the Universidad San Francisco de Quito. We thank EMOV EP and ETAPA EP, municipal entities that provided the meteorological and quality records.

Conflicts of Interest: The authors declare no conflicts of interest.

Abbreviations

 doi:10.20944/preprints202511.1436.v1

The following abbreviations are used in this manuscript:

EDGAR	The Emissions Database for Global Atmospheric Research dataset
EI 2021	The emissions inventory of Cuenca for the year 2021, assessed in this manuscript
EMOV EP	Empresa Pública Municipal de Movilidad, Tránsito y Transporte de Cuenca
ETAPA EP	Empresa Pública Municipal de Telecomunicaciones, Agua Potable, Alcantarillado y Saneamiento
GHGs	Greenhouse gases
IPCC	Intergovernmental Panel on Climate Change
RTV	Revisión Técnica Vehicular
SGDs	Sustainable Development Goals
WRF-Chem	The Weather Research and Forecasting with Chemistry model

References

1. van Aardenne, J. A. Uncertainties in Emission Inventories, Wageningen University, 2002. https://doi.org/10.18174/198412.
2. Molina, M. J.; Molina, L. T. Megacities and Atmospheric Pollution. *Journal of the Air & Waste Management Association* **2004**, *54* (6), 644–680. https://doi.org/10.1080/10473289.2004.10470936.
3. Baklanov, A.; Molina, L. T.; Gauss, M. Megacities, Air Quality and Climate. *Atmospheric Environment* **2016**, *126*, 235–249. https://doi.org/10.1016/j.atmosenv.2015.11.059.
4. European Commission. Joint Research Centre. *GHG Emissions of All World Countries: 2025.*; Publications Office: LU, 2025.
5. Deroubaix, A.; Hoelzemann, J. J.; Ynoue, R. Y.; Toledo de Almeida Albuquerque, T.; Alves, R. C.; de Fatima Andrade, M.; Andreão, W. L.; Bouarar, I.; de Souza Fernandes Duarte, E.; Elbern, H.; Franke, P.; Lange, A. C.; Lichtig, P.; Lugon, L.; Martins, L. D.; de Arruda Moreira, G.; Pedruzzi, R.; Rosario, N.; Brasseur, G. Intercomparison of Air Quality Models in a Megacity: Toward an Operational Ensemble Forecasting System for São Paulo. *Journal of Geophysical Research: Atmospheres* **2024**, *129* (1), e2022JD038179. https://doi.org/10.1029/2022JD038179.
6. Acdan, J. J. M.; Pierce, R. B.; Kuang, S.; McKinney, T.; Stevenson, D.; Newchurch, M. J.; Pfister, G.; Ma, S.; Tong, D. Evaluation of WRF-Chem Air Quality Forecasts during the AEROMMA and STAQS 2023 Field Campaigns. *J Air Waste Manag Assoc* **2024**, *74* (11), 783–803. https://doi.org/10.1080/10962247.2024.2380333.
7. Georgiou, G. K.; Christoudias, T.; Proestos, Y.; Kushta, J.; Pikridas, M.; Sciare, J.; Savvides, C.; Lelieveld, J. Evaluation of WRF-Chem Model (v3.9.1.1) Real-Time Air Quality Forecasts over the Eastern Mediterranean. *Geoscientific Model Development* **2022**, *15* (10), 4129–4146. https://doi.org/10.5194/gmd-15-4129-2022.
8. *Full article: Modeling emissions for three-dimensional atmospheric chemistry transport models*. https://www.tandfonline.com/doi/full/10.1080/10962247.2018.1424057 (accessed 2025-11-11).
9. *THE 17 GOALS | Sustainable Development*. https://sdgs.un.org/goals (accessed 2024-05-04).
10. *EDGAR - The Emissions Database for Global Atmospheric Research*. https://edgar.jrc.ec.europa.eu/emissions_data_and_maps?utm_source=chatgpt.com (accessed 2025-10-07).
11. *CAMS global emission inventories*. https://ads.atmosphere.copernicus.eu/datasets/cams-global-emission-inventories?tab=overview (accessed 2025-10-07).
12. Baklanov, A.; Zhang, Y. Advances in Air Quality Modeling and Forecasting. *Global Transitions* **2020**, *2*, 261–270. https://doi.org/10.1016/j.glt.2020.11.001.
13. Sokhi, R. S.; Moussiopoulos, N.; Baklanov, A.; Bartzis, J.; Coll, I.; Finardi, S.; Friedrich, R.; Geels, C.; Grönholm, T.; Halenka, T.; Ketzel, M.; Maragkidou, A.; Matthias, V.; Moldanova, J.; Ntziachristos, L.; Schäfer, K.; Suppan, P.; Tsegas, G.; Carmichael, G.; Franco, V.; Hanna, S.; Jalkanen, J.-P.; Velders, G. J. M.; Kukkonen, J. Advances in Air Quality Research – Current and Emerging Challenges. *Atmospheric Chemistry and Physics* **2022**, *22* (7), 4615–4703. https://doi.org/10.5194/acp-22-4615-2022.
14. Park, M.; Hu, H.; Kim, Y.; Fried, A.; Simpson, I. J.; Jin, H.; Weinheimer, A.; Huey, G.; Crawford, J.; Woo, J.-H. Evaluation of the Emission Inventory for Large Point Emission Sources in South Korea by Applying Measured Data from the NASA/NIER KORUS-AQ Aircraft Field Campaign. *Elementa: Science of the Anthropocene* **2023**, *11* (1), 00105. https://doi.org/10.1525/elementa.2022.00105.
15. Crippa, M.; Guizzardi, D.; Pagani, F.; Schiavina, M.; Melchiorri, M.; Pisoni, E.; Graziosi, F.; Muntean, M.; Maes, J.; Dijkstra, L.; Van Damme, M.; Clarisse, L.; Coheur, P. Insights into the Spatial Distribution of Global,

 doi:10.20944/preprints202511.1436.v1

National, and Subnational Greenhouse Gas Emissions in the Emissions Database for Global Atmospheric Research (EDGAR v8.0). *Earth System Science Data* **2024**, *16* (6), 2811–2830. https://doi.org/10.5194/essd-16-2811-2024.

16. Solazzo, E.; Crippa, M.; Guizzardi, D.; Muntean, M.; Choulga, M.; Janssens-Maenhout, G. Uncertainties in the Emissions Database for Global Atmospheric Research (EDGAR) Emission Inventory of Greenhouse Gases. *Atmospheric Chemistry and Physics* **2021**, *21* (7), 5655–5683. https://doi.org/10.5194/acp-21-5655-2021.
17. Malasani, C. R.; Swain, B.; Patel, A.; Pulipatti, Y.; Anchan, N. L.; Sharma, A.; Vountas, M.; Liu, P.; Gunthe, S. S. Modeling of Mercury Deposition in India: Evaluating Emission Inventories and Anthropogenic Impacts. *Environ. Sci.: Processes Impacts* **2024**, *26* (11), 1999–2009. https://doi.org/10.1039/D4EM00324A.
18. Baklanov, A.; Brunner, D.; Carmichael, G.; Flemming, J.; Freitas, S.; Gauss, M.; Hov, Ø.; Mathur, R.; Schlünzen, K. H.; Seigneur, C.; Vogel, B. Key Issues for Seamless Integrated Chemistry–Meteorology Modeling. *Bulletin of the American Meteorological Society* **2017**, *98* (11), 2285–2292. https://doi.org/10.1175/BAMS-D-15-00166.1.
19. Parra, R. *Inventario de Emisiones Atmosféricas Del Cantón Cuenca 2014*; 2016. https://doi.org/10.13140/RG.2.2.17665.66405.
20. Parra, R. Assessment of Land Surface Schemes from the WRF-Chem for Atmospheric Modeling in the Andean Region of Ecuador. *Atmosphere* **2023**, *14* (3), 508. https://doi.org/10.3390/atmos14030508.
21. Parra, R. Impact of Cumulus Options from Weather Research and Forecasting with Chemistry in Atmospheric Modeling in the Andean Region of Southern Ecuador. *Atmosphere* **2024**, *15* (6), 693. https://doi.org/10.3390/atmos15060693.
22. *EMOV*. https://caire.emov.gob.ec/ (accessed 2025-02-22).
23. *EMOV*. https://caire.emov.gob.ec/informes (accessed 2025-02-22).
24. World Health Organization. *WHO Global Air Quality Guidelines: Particulate Matter (PM2.5 and PM10), Ozone, Nitrogen Dioxide, Sulfur Dioxide and Carbon Monoxide*; World Health Organization, 2021.
25. Parra, R.; Molina, C.; Caguana, C.; Heredia, E. *Inventario de Emisiones Atmosféricas Del Cantón Cuenca 2021*; 2023.
26. *EMEP/EEA air pollutant emission inventory guidebook 2023*. https://www.eea.europa.eu/en/analysis/publications/emep-eea-guidebook-2023 (accessed 2025-02-13).
27. Guenther, A. B.; Zimmerman, P. R.; Harley, P. C.; Monson, R. K.; Fall, R. Isoprene and Monoterpene Emission Rate Variability: Model Evaluations and Sensitivity Analyses. *Journal of Geophysical Research: Atmospheres* **1993**, *98* (D7), 12609–12617. https://doi.org/10.1029/93JD00527.
28. Guenther, A.; Hewitt, C. N.; Erickson, D.; Fall, R.; Geron, C.; Graedel, T.; Harley, P.; Klinger, L.; Lerdau, M.; Mckay, W. A.; Pierce, T.; Scholes, B.; Steinbrecher, R.; Tallamraju, R.; Taylor, J.; Zimmerman, P. A Global Model of Natural Volatile Organic Compound Emissions. *Journal of Geophysical Research: Atmospheres* **1995**, *100* (D5), 8873–8892. https://doi.org/10.1029/94JD02950.
29. *TFI — IPCC*. https://www.ipcc.ch/working-group/tfi/ (accessed 2025-02-08).
30. Skamarock, W. C.; Klemp, J. B.; Dudhia, J.; Gill, D. O.; Barker, D. M.; Duda, M. G.; Huang, X.-Y.; Wang, W.; Powers, J. G. A Description of the Advanced Research WRF Version 3.
31. *CISL RDA: NCEP FNL Operational Model Global Tropospheric Analyses, continuing from July 1999*. https://rda.ucar.edu/datasets/ds083.2/ (accessed 2022-12-30).
32. Zaveri, R. A.; Peters, L. K. A New Lumped Structure Photochemical Mechanism for Large-Scale Applications. *J. Geophys. Res.* **1999**, *104* (D23), 30387–30415. https://doi.org/10.1029/1999JD900876.
33. Zaveri, R. A.; Easter, R. C.; Fast, J. D.; Peters, L. K. Model for Simulating Aerosol Interactions and Chemistry (MOSAIC). *J. Geophys. Res.* **2008**, *113* (D13), D13204. https://doi.org/10.1029/2007JD008782.
34. Hong, S.-Y.; Dudhia, J.; Chen, S.-H. A Revised Approach to Ice Microphysical Processes for the Bulk Parameterization of Clouds and Precipitation. *Mon. Wea. Rev.* **2004**, *132* (1), 103–120. https://doi.org/10.1175/1520-0493(2004)132<0103:ARATIM>2.0.CO;2.
35. Mlawer, E. J.; Taubman, S. J.; Brown, P. D.; Iacono, M. J.; Clough, S. A. Radiative Transfer for Inhomogeneous Atmospheres: RRTM, a Validated Correlated-k Model for the Longwave. *J. Geophys. Res.* **1997**, *102* (D14), 16663–16682. https://doi.org/10.1029/97JD00237.

 doi:10.20944/preprints202511.1436.v1

36. Chou, M.-D.; Suarez, M. J. *A Solar Radiation Parameterization for Atmospheric Studies*; NASA/TM-1999-104606/VOL15; 1999. https://ntrs.nasa.gov/citations/19990060930 (accessed 2022-12-30).
37. Paulson, C. A. The Mathematical Representation of Wind Speed and Temperature Profiles in the Unstable Atmospheric Surface Layer. *J. Appl. Meteor.* **1970**, *9* (6), 857–861. https://doi.org/10.1175/1520-0450(1970)009<0857:TMROWS>2.0.CO;2.
38. Hong, S.-Y.; Noh, Y.; Dudhia, J. A New Vertical Diffusion Package with an Explicit Treatment of Entrainment Processes. *Monthly Weather Review* **2006**, *134* (9), 2318–2341. https://doi.org/10.1175/MWR3199.1.
39. Chen, F.; Dudhia, J. Coupling an Advanced Land Surface–Hydrology Model with the Penn State–NCAR MM5 Modeling System. Part II: Preliminary Model Validation. *Mon. Wea. Rev.* **2001**, *129* (4), 587–604. https://doi.org/10.1175/1520-0493(2001)129<0587:CAALSH>2.0.CO;2.
40. *The application of models under the European Union's Air Quality Directive: A technical reference guide — European Environment Agency*. https://www.eea.europa.eu/publications/fairmode (accessed 2022-12-30).
41. *Rain day - Glossary of Meteorology*. https://glossary.ametsoc.org/wiki/Rain_day (accessed 2023-11-21).
42. *Acuerdo Nº 97/A - Norma de calidad del aire ambiente o nivel de inmisión (Anexo 4, Libro VI de la Calidad Ambiental, del Texto Unificado de la Legislación Secundaria del Ministerio del Ambiente).* | *FAOLEX*. https://www.fao.org/faolex/results/details/es/c/LEX-FAOC155133/ (accessed 2024-07-25).
43. *Air Quality Guidelines: Global Update 2005: Particulate Matter, Ozone, Nitrogen Dioxide, and Sulfur Dioxide*; World Health Organization, Ed.; World Health Organization: Copenhagen, Denmark, 2006.
44. Simon, H.; Baker, K. R.; Phillips, S. Compilation and Interpretation of Photochemical Model Performance Statistics Published between 2006 and 2012. *Atmospheric Environment* **2012**, *61*, 124–139. https://doi.org/10.1016/j.atmosenv.2012.07.012.
45. Crippa, M.; Solazzo, E.; Huang, G.; Guizzardi, D.; Koffi, E.; Muntean, M.; Schieberle, C.; Friedrich, R.; Janssens-Maenhout, G. High Resolution Temporal Profiles in the Emissions Database for Global Atmospheric Research. *Sci Data* **2020**, *7* (1), 121. https://doi.org/10.1038/s41597-020-0462-2.
46. Intergovernmental Panel on Climate Change (IPCC). *Climate Change 2021 – The Physical Science Basis: Working Group I Contribution to the Sixth Assessment Report of the Intergovernmental Panel on Climate Change*, 1st ed.; Cambridge University Press, 2023. https://doi.org/10.1017/9781009157896.
47. Gao, Z.; Zhou, X. A Review of the CAMx, CMAQ, WRF-Chem and NAQPMS Models: Application, Evaluation and Uncertainty Factors. *Environmental Pollution* **2024**, *343*, 123183. https://doi.org/10.1016/j.envpol.2023.123183.
48. Qi, Z.; Gu, M.; Cao, J.; Zhang, Z.; You, C.; Zhan, Y.; Ma, Z.; Huang, W. The Effects of Varying Altitudes on the Rates of Emissions from Diesel and Gasoline Vehicles Using a Portable Emission Measurement System. *Atmosphere* **2023**, *14* (12), 1739. https://doi.org/10.3390/atmos14121739.
49. Jiang, Z.; Wu, L.; Niu, H.; Jia, Z.; Qi, Z.; Liu, Y.; Zhang, Q.; Wang, T.; Peng, J.; Mao, H. Investigating the Impact of High-Altitude on Vehicle Carbon Emissions: A Comprehensive on-Road Driving Study. *Science of The Total Environment* **2024**, *918*, 170671. https://doi.org/10.1016/j.scitotenv.2024.170671.
50. Jaworski, A.; Kuszewski, H.; Ustrzycki, A.; Balawender, K.; Lejda, K.; Woś, P. Analysis of the Repeatability of the Exhaust Pollutants Emission Research Results for Cold and Hot Starts under Controlled Driving Cycle Conditions. *Environ Sci Pollut Res* **2018**, *25* (18), 17862–17877. https://doi.org/10.1007/s11356-018-1983-5.
51. Valverde, V.; Mora, B. A.; Clairotte, M.; Pavlovic, J.; Suarez-Bertoa, R.; Giechaskiel, B.; Astorga-LLorens, C.; Fontaras, G. Emission Factors Derived from 13 Euro 6b Light-Duty Vehicles Based on Laboratory and On-Road Measurements. *Atmosphere* **2019**, *10* (5), 243. https://doi.org/10.3390/atmos10050243.
52. Park, G.; Mun, S.; Hong, H.; Chung, T.; Jung, S.; Kim, S.; Seo, S.; Kim, J.; Lee, J.; Kim, K.; Park, T.; Kang, S.; Ban, J.; Yu, D.-G.; Woo, J.-H.; Lee, T. Characterization of Emission Factors Concerning Gasoline, LPG, and Diesel Vehicles via Transient Chassis-Dynamometer Tests. *Applied Sciences* **2019**, *9* (8), 1573. https://doi.org/10.3390/app9081573.
53. Kousoulidou, M.; Fontaras, G.; Ntziachristos, L.; Bonnel, P.; Samaras, Z.; Dilara, P. Use of Portable Emissions Measurement System (PEMS) for the Development and Validation of Passenger Car Emission Factors. *Atmospheric Environment* **2013**, *64*, 329–338. https://doi.org/10.1016/j.atmosenv.2012.09.062.

 doi:10.20944/preprints202511.1436.v1

54. Rivera-Campoverde, N. D.; Muñoz-Sanz, J. L.; Arenas-Ramirez, B. del V. Estimation of Pollutant Emissions in Real Driving Conditions Based on Data from OBD and Machine Learning. *Sensors* **2021**, *21* (19), 6344. https://doi.org/10.3390/s21196344.
55. Perdikopoulos, M.; Karageorgiou, T.; Ntziachristos, L.; Deville Cavellin, L.; Joly, F.; Vigneron, J.; Arfire, A.; Debert, C.; Sanchez, O.; Gaie-Levrel, F.; Marfaing, H. Developing Emission Factors from Real-World Emissions of Euro VI Urban Diesel, Diesel-Hybrid, and Compressed Natural Gas Buses. *Atmosphere* **2025**, *16* (3), 293. https://doi.org/10.3390/atmos16030293.
56. Clark, N. N.; Gautam, M. Evaluation of Technology to Support A Heavy-Duty Diesel Vehicle Inspection And Maintenance Program.
57. Yang, H.-H.; Kumar, A.; Dhital, N. B.; Wang, L.-C.; Wu, C.-H.; Kamyab, H.; Yusuf, M. Evaluating the Feasibility of Estimating Particulate Mass Emissions of Older-Model Diesel Vehicle Using Smoke Opacity Measurements. *Sci Rep* **2024**, *14*, 31494. https://doi.org/10.1038/s41598-024-83327-1.
58. Bracho-Nunez, A.; Welter, S.; Staudt, M.; Kesselmeier, J. Plant-Specific Volatile Organic Compound Emission Rates from Young and Mature Leaves of Mediterranean Vegetation. *Journal of Geophysical Research: Atmospheres* **2011**, *116* (D16). https://doi.org/10.1029/2010JD015521.
59. Laguerre, A.; Brennan, D. L.; Starry, O.; Rosenstiel, T. N.; Gall, E. T. Characterization of Volatile Organic Compound Emissions and CO2 Uptake from Eco-Roof Plants. *Building and Environment* **2023**, *234*, 110158. https://doi.org/10.1016/j.buildenv.2023.110158.
60. Cazorla, M.; Parra, R.; Herrera, E.; da Silva, F. R. Characterizing Ozone throughout the Atmospheric Column over the Tropical Andes from in Situ and Remote Sensing Observations. *Elementa: Science of the Anthropocene* **2021**, *9* (1), 00019. https://doi.org/10.1525/elementa.2021.00019.
61. *Rainfall and Cloud Dynamics in the Andes: A Southern Ecuador Case Study*. https://www.hindawi.com/journals/amete/2016/3192765/ (accessed 2023-12-21).
62. Yarragunta, Y.; Francis, D.; Fonseca, R.; Nelli, N. Evaluation of the WRF-Chem Performance for the Air Pollutants over the United Arab Emirates. *Atmospheric Chemistry and Physics* **2025**, *25* (3), 1685–1709. https://doi.org/10.5194/acp-25-1685-2025.